Signal Processing 108 (2015) 389–399

Contents lists available at ScienceDirect

Signal Processing

journal homepage: www.elsevier.com/locate/sigpro

Signal detection with noisy reference for passive sensing ☆

Guolong Cui [a], Jun Liu [a], Hongbin Li [a,*], Braham Himed [b]

[a] Department of Electrical and Computer Engineering, Stevens Institute of Technology, Hoboken, NJ 07030, USA
[b] AFRL/RYMD, 2241 Avionics Circle, Bldg 620, Dayton, OH 45433, USA

ARTICLE INFO

Article history:
Received 30 April 2014
Received in revised form
6 August 2014
Accepted 25 September 2014
Available online 8 October 2014

Keywords:
Cross-correlation detector
Generalized likelihood ratio test (GLRT)
Matched filter detector
Reference signal

ABSTRACT

In many detection applications, the signal to be detected, referred to as *target signal*, is not directly available. A reference channel (RC) is often deployed to collect a noise-contaminated version of the target signal to serve as a reference, which is then used to assist detecting the presence/absence of the target signal in a test channel (TC). A standard approach is to cross-correlate (CC) the signals received in the TC and RC, respectively. When the signal-to-noise ratio (SNR) in the RC is high, the CC behaves like the optimum matched filter. However, when the SNR in the RC is low, the CC detector suffers significant degradation. This paper considers the above detection problem with a noisy reference signal. We propose four detectors based on the generalized likelihood ratio test principle, by treating the unknown target signal to be deterministic or stochastic and under conditions whether the noise variance is known or unknown. Our results demonstrate that the noise in the RC has an impact on the achievable detection performance. However, when the reference signal is noisy, three of the proposed detectors offer substantial improvements in detection performance over the CC detector.

1. Introduction

Detection of a signal in noise has been a topic of long-standing interest in sensing and communications. If the signal to be detected is perfectly known and the noise is stationary with zero-mean and white power spectral density, the optimal detector is the matched filter (MF) which maximizes the output signal-to-noise ratio (SNR) [1]. However, the signal may not be known in many practical applications, such as underwater acoustics [2–5], seismology [6–9], neurophysiology [10,11], and passive radar [12–16]. Consider for example passive radar. Unlike its active counterpart, a passive radar does not transmit a known waveform and then listen for echos. Instead, it utilizes commercial RF signals from TV stations or cellular towers as sources to illuminate potential targets of interest. The RF source waveforms are generally unknown to the passive radar receiver.

A conventional approach to the unknown signal detection problem is to deploy a reference channel (RC) for collecting the unknown transmitted signal to serve as a reference. In passive radar, a reference signal can be obtained by using a directive antenna pointing toward the commercial RF source with a known location. Given the availability of the reference signal, a natural solution is to mimic the MF processing, i.e., cross-correlate (CC) the reference and the test signal observed in a test channel (TC). Nevertheless, the reference signal is inevitably contaminated by noise. Under the condition that the SNR in the RC is high, the noise is negligible and the CC detector behaves like the MF. However, the detection performance of the CC detector would be significantly degraded, when

☆ This work was supported in part by a subcontract with Dynetics, Inc. for research sponsored by the Air Force Research Laboratory (AFRL) under Contract FA8650-08-D-1303.

* Corresponding author.
E-mail addresses: guolongcui@gmail.com (G. Cui), jun_liu_math@hotmail.com (J. Liu), Hongbin.Li@stevens.edu (H. Li), braham.himed@us.af.mil (B. Himed).

http://dx.doi.org/10.1016/j.sigpro.2014.09.034
0165-1684/

the SNR in the RC is low. In such cases, improved detection performance is possible, if the noise in the reference signal is properly taken into account. In this paper, we consider signal detection with a noisy reference.

Specifically, the detection problem in the presence of a noisy reference signal can be formulated as the following binary hypothesis test:

$$H_0: \begin{cases} \boldsymbol{x}_r = \beta \boldsymbol{s} + \boldsymbol{v}, \\ \boldsymbol{x}_t = \boldsymbol{w}, \end{cases} \tag{1a}$$

$$H_1: \begin{cases} \boldsymbol{x}_r = \beta \boldsymbol{s} + \boldsymbol{v}, \\ \boldsymbol{x}_t = \alpha \boldsymbol{s} + \boldsymbol{w}, \end{cases} \tag{1b}$$

where $\boldsymbol{x}_r$ and $\boldsymbol{x}_t$ denote $N \times 1$ vectors composed of complex (baseband equivalent) samples received in the RC and TC, respectively; $\boldsymbol{s}$ is an $N \times 1$ vector containing samples of the unknown transmitted signal waveform; α and β are unknown scaling parameters accounting for the channel propagation effects; $\boldsymbol{w}$ and $\boldsymbol{v}$ are noise vectors in the TC and RC, respectively, which are modeled as independent circular[1] complex Gaussian vectors with zero mean and covariance matrix $\eta \mathbf{I}_N$, where η denotes the noise power and $\mathbf{I}_N$ stands for an N-dimensional identity matrix. The problem of interest is to decide between hypotheses H_1 and H_0 given observations of $\boldsymbol{x}_r$ and $\boldsymbol{x}_t$ made over the RC and TC channels.

We employ two models to describe the unknown transmitted signal $\boldsymbol{s}$, namely, a deterministic model where $\boldsymbol{s}$ is deterministic but unknown, and a stochastic model in which $\boldsymbol{s}$ is a complex Gaussian vector. The stochastic model is suitable for signal sources involving multiplexing techniques, such as the orthogonal frequency division multiplexing (OFDM) as used in digital audio broadcasting [17], which use multiple random information streams to form a composite communication signal that can be adequately modeled as a Gaussian process due to the central limit theorem (CLT).

In this paper, we develop four generalized likelihood ratio test (GLRT) detectors for both models under the assumption of known and unknown noise power. In particular, cyclic iteration algorithms are proposed to obtain the maximum likelihood estimates (MLEs) of unknown parameters. Numerical simulations are presented to illustrate the detection performance of these proposed detectors. It is shown that the proposed GLRT detectors, except the one developed under the assumption of unknown noise power in the stochastic model, outperforms the CC detector, especially when the noise in the RC is not negligible.

A comment on the model in (1) for passive sensing is now in order. In passive radar, since the target location is unknown, there is an unknown delay of the waveform $\boldsymbol{s}$ observed at the TC relative to that observed at the RC. In practical sensing scenarios, the delay is within a known interval (i.e., the target is located within a range specified by a minimum and a maximum detection distance), which is discretized into a number of small sub-intervals called *range bins*. The hypothesis in (1) is tested on each bin one by one, whereby the RC and TC observations are aligned according to the delay of the tested range bin and detection is performed by using, e.g., any detector discussed in this paper. Presumably, the test result will be positive with a high probability only when the tested range bin matches the true unknown delay. For simplicity (and also as in the standard radar signal detection literature), we assume that the delay alignment has already been accomplished, and the observations in (1) have already been delay compensated. Likewise, when detecting a moving target, there is a Doppler uncertainty which can be handled by discretizing the Doppler frequency into Doppler bins and running the test on each Doppler bin one by one. It should be noted that delay and Doppler uncertainties are present in active radar as well, and they are often handled in a similar manner there.

The remainder of the paper is organized as follows. In Section 2, two GLRT-based detectors are devised under the deterministic model. In Section 3, we design two GLRT-based detectors under the stochastic model. In Section 4, computer simulations are offered. Finally, we provide concluding remarks and possible future research tracks in Section 5.

Notation: Vectors (matrices) are denoted by boldface lower (upper) case letters. Superscripts $(\cdot)^T$, $(\cdot)^*$, and $(\cdot)^\dagger$ denote transpose, complex conjugate, and complex conjugate transpose, respectively. $\mathbf{I}_p$ stands for a p-dimensional identity matrix. $\|\cdot\|$ is the Frobenius norm. $|\cdot|$, $\angle(\cdot)$, and $\Re(\cdot)$ denote the modulus, the phase, and the real part of a complex number, respectively. $\lambda_{\max}(\cdot)$ and $\lambda_{\min}(\cdot)$ represent the largest eigenvalue and the smallest eigenvalue of an argument, respectively. $\det(\cdot)$ denotes the determinant operation. $\mathrm{var}(\cdot)$ and $E(\cdot)$ are the variance and the statistical expectation, respectively. $\Pr\{\cdot\}$ denotes the probability of a random variable.

2. Deterministic model based detectors

The *Neyman–Pearson* criterion is widely used for signal detection, which enables us to obtain the maximum probability of detection while not allowing the probability of false alarm to exceed a certain value [1]. According to the *Neyman–Pearson* criterion, the optimum solution to the hypothesis testing problem in (1) is obtained by comparing the ratio of the likelihood of the received data under hypothesis over that under hypothesis with an appropriate detection threshold, i.e.,

$$\Lambda(\boldsymbol{x}_t, \boldsymbol{x}_r) = \frac{f_{H_1}(\boldsymbol{x}_t, \boldsymbol{x}_r)}{f_{H_0}(\boldsymbol{x}_t, \boldsymbol{x}_r)} \underset{H_0}{\overset{H_1}{\gtrless}} \gamma, \tag{2}$$

where $f_{H_0}(\boldsymbol{x}_t, \boldsymbol{x}_r)$ and $f_{H_1}(\boldsymbol{x}_t, \boldsymbol{x}_r)$ are the likelihood functions under H_0 and H_1, respectively, and γ denotes the detection threshold. Based on the Gaussian assumptions on $\boldsymbol{v}$ and $\boldsymbol{w}$, the probability density functions (PDFs) for deterministic $\boldsymbol{s}$ can be written as

$$f_{H_0}(\boldsymbol{x}_t, \boldsymbol{x}_r) = \frac{1}{\pi^{2N}\eta^{2N}} \exp\left(-\frac{\|\boldsymbol{x}_r - \beta \boldsymbol{s}\|^2 + \|\boldsymbol{x}_t\|^2}{\eta} \right), \tag{3}$$

and

$$f_{H_1}(\boldsymbol{x}_t, \boldsymbol{x}_r) = \frac{1}{\pi^{2N}\eta^{2N}} \exp\left(-\frac{\|\boldsymbol{x}_r - \beta \boldsymbol{s}\|^2 + \|\boldsymbol{x}_t - \alpha \boldsymbol{s}\|^2}{\eta} \right), \tag{4}$$

[1] A circular complex random variable indicates that its real part and imaginary part are independent and identically distributed random variables.

under H_0 and H_1, respectively. For notational simplicity, the dependence of the PDFs $f_{H_0}(\boldsymbol{x}_t,\boldsymbol{x}_r)$ and $f_{H_1}(\boldsymbol{x}_t,\boldsymbol{x}_r)$ on unknown parameters is suppressed. Similar notation will be adopted throughout this paper.

Let us examine the unknown parameters in the detection problem. The channel parameters α and β and the transmitted waveform $\boldsymbol{s}$ are generally unknown. However, the noise variance η may or may not be known depending on if a prior calibration/measurement is available. The noise may include the receiver thermal noise which can be easily measured [18], and/or the external noise which can be estimated in a way similar to that in cognitive radio, i.e., by measuring the power level of a channel which is known to be idle [19].

The LRT (2) cannot be implemented due to the presence of unknown parameters. We consider the generalized LRT (GLRT), which is equivalent to replacing the unknown parameters with their MLEs. In the following, we develop two GLRT detectors with known and unknown η, by assuming that α, β, and $\boldsymbol{s}$ are deterministic but unknown.

2.1. GLRT with known noise power η

First, we examine the case of known η. The GLRT detector can be obtained as

$$\frac{\max_{\{\alpha,\beta,\boldsymbol{s}\}} f_{H_1}(\boldsymbol{x}_t,\boldsymbol{x}_r)}{\max_{\{\beta,\boldsymbol{s}\}} f_{H_0}(\boldsymbol{x}_t,\boldsymbol{x}_r)} \underset{H_0}{\overset{H_1}{\gtrless}} \gamma_1. \tag{5}$$

Taking the logarithm of (5) leads to

$$\max_{\{\alpha,\beta,\boldsymbol{s}\}} \ell_1 - \max_{\{\beta,\boldsymbol{s}\}} \ell_0 \underset{H_0}{\overset{H_1}{\gtrless}} \ln \gamma_1, \tag{6}$$

where $\ell_1 = \ln f_{H_1}$ and $\ell_0 = \ln f_{H_0}$. As derived in Appendix A, the MLEs of α and β conditioned on $\boldsymbol{s}$ under H_1 are, respectively,

$$\hat{\alpha}_1 = \frac{\boldsymbol{s}^\dagger \boldsymbol{x}_t}{\boldsymbol{s}^\dagger \boldsymbol{s}} \quad \text{and} \quad \hat{\beta}_1 = \frac{\boldsymbol{s}^\dagger \boldsymbol{x}_r}{\boldsymbol{s}^\dagger \boldsymbol{s}}. \tag{7}$$

The MLE of $\boldsymbol{s}$ under H_1 is the eigenvector corresponding to the largest eigenvalue of the matrix $\mathbf{F}_1 = \boldsymbol{x}_r\boldsymbol{x}_r^\dagger + \boldsymbol{x}_t\boldsymbol{x}_t^\dagger$. It should be pointed out that there exists an ambiguity in the norm of the vector $\boldsymbol{s}$, due to the multiplicative relation between the unknown α or β and $\boldsymbol{s}$. Therefore, $\|\boldsymbol{s}\|$ cannot be uniquely determined. Nevertheless, this ambiguity does not affect the GLRT. Substituting these MLEs into ℓ_1 results in

$$\max_{\{\alpha,\beta,\boldsymbol{s}\}} \ell_1 = -2N\ln\pi - 2N\ln\eta - \frac{\|\boldsymbol{x}_t\|^2 + \|\boldsymbol{x}_r\|^2 - \sqrt{(\|\boldsymbol{x}_t\|^2 - \|\boldsymbol{x}_r\|^2)^2 + 4|\boldsymbol{x}_t^\dagger \boldsymbol{x}_r|^2}}{2\eta}. \tag{8}$$

In a similar way, the MLE of $\boldsymbol{s}$ under H_0 is the eigenvector corresponding to the largest eigenvalue of the matrix $\mathbf{F}_2 = \boldsymbol{x}_r\boldsymbol{x}_r^\dagger$. The MLE of β under H_0 is the same as that under H_1. Taking these MLEs into ℓ_0 yields

$$\max_{\{\beta,\boldsymbol{s}\}} \ell_0 = -2N\ln\pi - 2N\ln\eta - \frac{1}{\eta}\|\boldsymbol{x}_t\|^2. \tag{9}$$

Substituting (8) and (9) into (6), and after some algebraic manipulations, the GLRT can be finally obtained as

$$T_1 = \frac{1}{\eta}\left(\|\boldsymbol{x}_t\|^2 - \|\boldsymbol{x}_r\|^2 + \sqrt{(\|\boldsymbol{x}_t\|^2 - \|\boldsymbol{x}_r\|^2)^2 + 4|\boldsymbol{x}_t^\dagger \boldsymbol{x}_r|^2}\right) \underset{H_0}{\overset{H_1}{\gtrless}} \gamma_1', \tag{10}$$

where γ_1' is a suitably modified version of the threshold in (5). It is noted that the above detector is similar to the detector recently introduced in [20].

2.2. GLRT with unknown noise power η

Consider the case of unknown η, where the GLRT detector can be written as

$$\frac{\max_{\{\alpha,\beta,\boldsymbol{s},\eta\}} f_{H_1}(\boldsymbol{x}_t,\boldsymbol{x}_r)}{\max_{\{\beta,\boldsymbol{s},\eta\}} f_{H_0}(\boldsymbol{x}_t,\boldsymbol{x}_r)} \underset{H_0}{\overset{H_1}{\gtrless}} \gamma_2. \tag{11}$$

Taking the logarithm of (11) produces

$$\max_{\{\alpha,\beta,\boldsymbol{s},\eta\}} \ell_1 - \max_{\{\beta,\boldsymbol{s},\eta\}} \ell_0 \underset{H_0}{\overset{H_1}{\gtrless}} \ln \gamma_2. \tag{12}$$

Further development requires the MLEs of the unknown parameters under each hypothesis. These MLEs are given next.

It is obvious that under H_1,

$$\max_{\{\alpha,\beta,\boldsymbol{s},\eta\}} \ell_1 = \max_{\{\eta\}}\left\{\max_{\{\alpha,\beta,\boldsymbol{s}\}} \ell_1\right\}. \tag{13}$$

Using (8), we can show that the MLE of η under H_1 is

$$\hat{\eta}_1 = \frac{\|\boldsymbol{x}_t\|^2 + \|\boldsymbol{x}_r\|^2 - \sqrt{(\|\boldsymbol{x}_t\|^2 - \|\boldsymbol{x}_r\|^2)^2 + 4|\boldsymbol{x}_t^\dagger \boldsymbol{x}_r|^2}}{4N}. \tag{14}$$

Replacing η in (8) with its MLE $\hat{\eta}_1$ under H_1 leads to

$$\max_{\{\alpha,\beta,\boldsymbol{s},\eta\}} \ell_1 = -2N\ln\pi - 2N\ln\hat{\eta}_1 - 2N. \tag{15}$$

In a similar way, we have

$$\max_{\{\beta,\boldsymbol{s},\eta\}} \ell_0 = \max_{\{\eta\}}\left\{\max_{\{\beta,\boldsymbol{s}\}} \ell_0\right\}. \tag{16}$$

Applying (9), we obtain the MLE of η as

$$\hat{\eta}_0 = \frac{1}{2N}\|\boldsymbol{x}_t\|^2. \tag{17}$$

Accordingly,

$$\max_{\{\beta,\boldsymbol{s},\eta\}} \ell_0 = -2N\ln\pi - 2N\ln\hat{\eta}_0 - 2N. \tag{18}$$

Substituting (15) and (18) into (12) followed by simple manipulations, we obtain the GLRT for the case of unknown noise level as

$$T_2 = \frac{\|\boldsymbol{x}_t\|^2}{\|\boldsymbol{x}_t\|^2 + \|\boldsymbol{x}_r\|^2 - \sqrt{(\|\boldsymbol{x}_t\|^2 - \|\boldsymbol{x}_r\|^2)^2 + 4|\boldsymbol{x}_t^\dagger \boldsymbol{x}_r|^2}} \underset{H_0}{\overset{H_1}{\gtrless}} \gamma_2', \tag{19}$$

where γ_2' is a suitably modified version of the threshold in (11).

3. Stochastic model based detectors

The previous section has considered the GLRT design by treating the transmitted signal $\boldsymbol{s}$ to be deterministic but unknown. In some cases, it is possible to obtain

some partial information of $\boldsymbol{s}$, i.e., its statistical property. For instance, the signal from a multicarrier/OFDM modulation based transmitter is often modeled as a Gaussian process due to the CLT [21]. In the following, the samples $s(n)$ for $n=0,\ldots,N-1$ are modeled as independent and identically distributed (i.i.d.) circular complex Gaussian random variables with zero-mean and unit variance. Note that the variance of $s(n)$ can be absorbed by the channel parameters α and β. Hence, there is no loss of generality to assume that $s(n)$ has unit variance. In such a model, the PDF of $\boldsymbol{s}$ is

$$f(\boldsymbol{s})=\frac{1}{\pi^N}\exp(-\|\boldsymbol{s}\|^2). \tag{20}$$

Define

$$\alpha=a\exp(j\phi_1) \quad \text{and} \quad \beta=b\exp(j\phi_2). \tag{21}$$

Then, the likelihood function for random $\boldsymbol{s}$ under H_0 can be obtained by averaging (3) over $\boldsymbol{s}$, i.e.,

$$\begin{aligned} f^{\mathrm{s}}_{H_0}(\boldsymbol{x}_t,\boldsymbol{x}_r)&=\int f_{H_0}(\boldsymbol{x}_t,\boldsymbol{x}_r)f(\boldsymbol{s})\,d\boldsymbol{s}\\ &=\frac{1}{\pi^{2N}\eta^N(b^2+\eta)^N}\\ &\quad\times\exp\left(-\frac{(b^2+\eta)\|\boldsymbol{x}_t\|^2+\eta\|\boldsymbol{x}_r\|^2}{\eta(b^2+\eta)}\right), \end{aligned} \tag{22}$$

where the superscript "s" means that the PDF is for the stochastic model. In a similar way, the likelihood function for andom $\boldsymbol{s}$ under H_1 can be obtained by averaging (4) over $\boldsymbol{s}$, i.e.,

$$\begin{aligned} f^{\mathrm{s}}_{H_1}(\boldsymbol{x}_t,\boldsymbol{x}_r)&=\frac{1}{\pi^{2N}\eta^N(a^2+b^2+\eta)^N}\\ &\quad\times\exp\left[-\frac{(b^2+\eta)\|\boldsymbol{x}_t\|^2+(a^2+\eta)\|\boldsymbol{x}_r\|^2-2ab\Re(e^{j\phi}\boldsymbol{x}_t^\dagger\boldsymbol{x}_r)}{\eta(a^2+b^2+\eta)}\right], \end{aligned} \tag{23}$$

where $\phi=\phi_1-\phi_2$ denotes the phase difference between α and β.

Obviously, the LRT in (2) cannot be implemented due to the unknown parameters a, b, and ϕ. In the following, we derive two GLRT detectors in two cases: known and unknown η.

3.1. GLRT with known noise power η

Assume that the noise power η is known a priori. Then, the GLRT can be expressed as

$$\frac{\max_{\{a,b,\phi\}} f^{\mathrm{s}}_{H_1}(\boldsymbol{x}_t,\boldsymbol{x}_r)}{\max_{\{b\}} f^{\mathrm{s}}_{H_0}(\boldsymbol{x}_t,\boldsymbol{x}_r)}\underset{H_0}{\overset{H_1}{\gtrless}}\gamma_3. \tag{24}$$

Under H_0, let

$$\frac{\partial\ln f^{\mathrm{s}}_{H_0}(\boldsymbol{x}_t,\boldsymbol{x}_r)}{\partial b}=0. \tag{25}$$

Substituting (22) into (25), and after some algebraic manipulations, the MLE of b can be obtained by

$$\hat{b}_0=\sqrt{\frac{\|\boldsymbol{x}_r\|^2}{N}-\eta}. \tag{26}$$

Under H_1, the numerator in the left-hand side of (24) can be computed as

$$\max_{\{a,b,\phi\}} f^{\mathrm{s}}_{H_1}(\boldsymbol{x}_t,\boldsymbol{x}_r)=\max_{\{a,b\}}\left\{g^{\mathrm{s}}_{H_1}\right\}, \tag{27}$$

where

$$g^{\mathrm{s}}_{H_1}=\max_{\{\phi\}} f^{\mathrm{s}}_{H_1}(\boldsymbol{x}_t,\boldsymbol{x}_r). \tag{28}$$

It is easy to obtain that the MLE of ϕ under H_1 is $\hat{\phi}=-\angle(\boldsymbol{x}_t^\dagger\boldsymbol{x}_r)$. Using this MLE, we have

$$\begin{aligned} g^{\mathrm{s}}_{H_1}&=\frac{1}{\pi^{2N}\eta^N(a^2+b^2+\eta)^N}\\ &\quad\times\exp\left(-\frac{(b^2+\eta)\|\boldsymbol{x}_t\|^2+(a^2+\eta)\|\boldsymbol{x}_r\|^2-2ab|\boldsymbol{x}_t^\dagger\boldsymbol{x}_r|}{\eta(a^2+b^2+\eta)}\right). \end{aligned} \tag{29}$$

As derived in Appendix C, the MLEs of a and b are the solutions to the following equations:

$$p(a|b,\eta)=0 \quad \text{and} \quad q(b|a,\eta)=0, \tag{30}$$

where $p(a|b,\eta)$ and $q(b|a,\eta)$ are given by, respectively,

$$\begin{aligned} p(a|b,\eta)&=N\eta a^3+b|\boldsymbol{x}_t^\dagger\boldsymbol{x}_r|a^2-b|\boldsymbol{x}_t^\dagger\boldsymbol{x}_r|(b^2+\eta)\\ &\quad+\left[(N\eta+\|\boldsymbol{x}_r\|^2-\|\boldsymbol{x}_t\|^2)(b^2+\eta)-\eta\|\boldsymbol{x}_r\|^2\right]a, \end{aligned} \tag{31}$$

and

$$\begin{aligned} q(b|a,\eta)&=N\eta b^3+a|\boldsymbol{x}_t^\dagger\boldsymbol{x}_r|b^2-a|\boldsymbol{x}_t^\dagger\boldsymbol{x}_r|(a^2+\eta)\\ &\quad+\left[(N\eta+\|\boldsymbol{x}_t\|^2-\|\boldsymbol{x}_r\|^2)(a^2+\eta)-\eta\|\boldsymbol{x}_t\|^2\right]b. \end{aligned} \tag{32}$$

Unfortunately, closed-form solutions to (30) are not available. In the following, we present a cyclic iteration algorithm to find them (similar cyclic algorithms for parameter estimation are employed in [22,23]). Specifically, at the mth iteration, we first compute $p(a_{m-1}|b_{m-1},\eta)$ and $q(b_{m-1}|a_{m-1},\eta)$, and their gradients $p'(a_{m-1}|b_{m-1},\eta)$ and $q'(b_{m-1}|a_{m-1},\eta)$, where

$$\begin{aligned} p'(a_{m-1}|b_{m-1},\eta)&=3N\eta a_{m-1}^2+2b_{m-1}|\boldsymbol{x}_t^\dagger\boldsymbol{x}_r|a_{m-1}\\ &\quad+(N\eta+\|\boldsymbol{x}_r\|^2-\|\boldsymbol{x}_t\|^2)(b_{m-1}^2+\eta)-\eta\|\boldsymbol{x}_r\|^2, \end{aligned} \tag{33}$$

and

$$\begin{aligned} q'(b_{m-1}|a_{m-1},\eta)&=3N\eta b_{m-1}^2+2a_{m-1}|\boldsymbol{x}_t^\dagger\boldsymbol{x}_r|b_{m-1}\\ &\quad+(N\eta+\|\boldsymbol{x}_t\|^2-\|\boldsymbol{x}_r\|^2)(a_{m-1}^2+\eta)-\eta\|\boldsymbol{x}_t\|^2. \end{aligned} \tag{34}$$

Next, we calculate the mth iteration values a_m and b_m using the Newton–Raphson method [24]. This process is repeated until convergence. We summarize this algorithm as follows:

Cyclic algorithm I.

Input: $\boldsymbol{x}_t$, $\boldsymbol{x}_r$ and η.

Output: The MLEs $\hat{a}$ and $\hat{b}$.

1. For $m=1$, initialize a and b as
$$a_1=\sqrt{\frac{\|\boldsymbol{x}_t\|^2}{N}-\eta} \quad \text{and} \quad b_1=\sqrt{\frac{\|\boldsymbol{x}_r\|^2}{N}-\eta}. \tag{35}$$
2. Let $m\leftarrow m+1$, using the Newton–Raphson method [24], the mth iteration values a_m and b_m can be computed as
$$\begin{cases} a_m=a_{m-1}-\dfrac{p(a_{m-1}|b_{m-1},\eta)}{p'(a_{m-1}|b_{m-1},\eta)},\\ b_m=b_{m-1}-\dfrac{q(b_{m-1}|a_{m-1},\eta)}{q'(b_{m-1}|a_{m-1},\eta)}, \end{cases} \tag{36}$$
respectively, where p, p', q, and q' are given in (31), (33), (32), and (34), respectively.

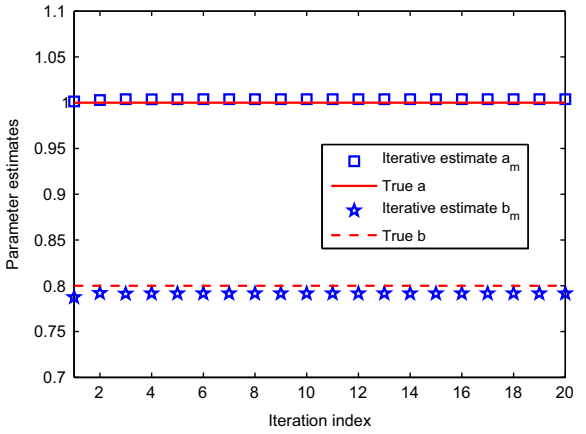

Fig. 1. Estimates of a_m and b_m versus iteration index for $M=100$, $N=100$, $a=1$, $b=0.8$, and $\eta=1$.

3. If $|a_m-a_{m-1}|\le\varepsilon$ and $|b_m-b_{m-1}|\le\varepsilon$, where ε is a parameter used to control convergence, output $\hat{a}=a_m$ and $\hat{b}=b_m$. Otherwise, repeat step 2 until convergence.

Notice that the above iterative algorithm might be sensitive to the initial values of a and b. In fact, there are three roots of $p(a|b,\eta)=0$ for a with given b and η (a similar phenomenon occurs with b for given a and η). Therefore, it is possible to converge to different local roots for different initial values. In practice, care should be taken when selecting the initial values a_1 and b_1. The intuitive selection for the initialization of a (or b) is its MLE only using $\boldsymbol{x}_t$ (or $\boldsymbol{x}_r$), i.e. (35). Numerical simulations in the following demonstrate that these initializations of a and b enable us to obtain satisfactory solutions.

The average MLEs of a and b obtained by the Cyclic algorithm I with $M=100$ independent experiments are presented in Fig. 1, where the true values $a=1$, $b=0.8$, $\eta=1$ and the samples $s(n)$ for $n=0,\ldots,N-1$ are independently selected from the circular complex Gaussian distribution with zero mean and unit variance. It can be observed that the proposed cyclic iteration algorithm can obtain satisfactory estimates close to the true a and b in several iterations.

So far, the estimates of a, b, ϕ are assumed to have already been obtained. Applying these estimates to (24), we obtain the GLRT detector for the stochastic model to be

$$L_1=\frac{\|\boldsymbol{x}_r\|^{2N}}{(\hat{a}^2+\hat{b}^2+\eta)^N}\times\exp\left(\frac{\|\boldsymbol{x}_t\|^2\hat{a}^2-(\hat{a}^2+\eta)\|\boldsymbol{x}_r\|^2+2\hat{a}\hat{b}|\boldsymbol{x}_t^\dagger\boldsymbol{x}_r|}{\eta(\hat{a}^2+\hat{b}^2+\eta)}\right)\underset{H_0}{\overset{H_1}{\gtrless}}\gamma_3', \tag{37}$$

where γ_3' is a suitably modified version of the threshold in (24).

3.2. GLRT with unknown noise power η

Here, we turn to the case of unknown η where the GLRT detector becomes

$$\frac{\max_{\{a,b,\phi,\eta\}}f_{H_1}^s(\boldsymbol{x}_t,\boldsymbol{x}_r)}{\max_{\{b,\eta\}}f_{H_0}^s(\boldsymbol{x}_t,\boldsymbol{x}_r)}\underset{H_0}{\overset{H_1}{\gtrless}}\gamma_4. \tag{38}$$

Under H_0, let

$$\frac{\partial\ln f_{H_0}^s(\boldsymbol{x}_t,\boldsymbol{x}_r)}{\partial b}=0\quad\text{and}\quad\frac{\partial\ln f_{H_0}^s(\boldsymbol{x}_t,\boldsymbol{x}_r)}{\partial\eta}=0. \tag{39}$$

Substituting (22) into (39), we obtain the MLEs of b and η as, respectively,

$$\hat{\eta}_0=\frac{\|\boldsymbol{x}_t\|^2}{N}\quad\text{and}\quad\hat{b}_0=\sqrt{\frac{\|\boldsymbol{x}_r\|^2-\|\boldsymbol{x}_t\|^2}{N}}. \tag{40}$$

Under H_1, the numerator in the left-hand side of (38) can be computed as

$$\max_{\{a,b,\phi,\eta\}}f_{H_1}^s(\boldsymbol{x}_t,\boldsymbol{x}_r)=\max_{\{a,b,\eta\}}\left\{g_{H_1}^s\right\}, \tag{41}$$

where $g_{H_1}^s$ is given in (29). In Appendix C, we derive the MLEs of a, b and η to be the solutions to the following equations:

$$p(a|b,\eta)=0,\quad q(b|a,\eta)=0\quad\text{and}\quad h(\eta|a,b)=0, \tag{42}$$

where $p(a|b,\eta)$ and $q(b|a,\eta)$ are defined in (31) and (32), respectively, $h(\eta|a,b)$ is given by

$$\begin{aligned}h(\eta|a,b)=2N\eta^3+\left(3Na^2+3Nb^2-\|\boldsymbol{x}_r\|^2-\|\boldsymbol{x}_t\|^2\right)\eta^2\\+\left[N(a^2+b^2)^2-2\left(b^2\|\boldsymbol{x}_t\|^2+a^2\|\boldsymbol{x}_r\|^2-2ab|\boldsymbol{x}_t^\dagger\boldsymbol{x}_r|\right)\right]\eta\\-\left(b^2\|\boldsymbol{x}_t\|^2+a^2\|\boldsymbol{x}_r\|^2-2ab|\boldsymbol{x}_t^\dagger\boldsymbol{x}_r|\right)(a^2+b^2).\end{aligned} \tag{43}$$

Unfortunately, (42) does not have a closed-form solution. Therefore, a cyclic iteration algorithm similar to that of Section 3.1 is proposed to obtain the MLEs of a, b, and η, which is summarized as follows:

Cyclic algorithm II.

Input: $\boldsymbol{x}_t$ and $\boldsymbol{x}_r$.

Output: The MLEs $\hat{a}$, $\hat{b}$, and $\hat{\eta}$.

1. For $m=1$, initialize a, b and η as

$$\eta_1=r_0,\quad a_1=\sqrt{\tfrac{\|\boldsymbol{x}_t\|^2}{N}-\eta_1},\quad b_1=\sqrt{\tfrac{\|\boldsymbol{x}_r\|^2}{N}-\eta_1}, \tag{44}$$

where r_0 is any positive real number.

2. Let $m\leftarrow m+1$, using the Newton–Raphson method [24], the mth iteration values a_m, b_m, and η_m can be respectively computed as

$$\begin{cases}a_m=a_{m-1}-\dfrac{p(a_{m-1}|b_{m-1},\eta_{m-1})}{p'(a_{m-1}|b_{m-1},\eta_{m-1})},\\ b_m=b_{m-1}-\dfrac{q(b_{m-1}|a_{m-1},\eta_{m-1})}{q'(b_{m-1}|a_{m-1},\eta_{m-1})},\\ \eta_m=\eta_{m-1}-\dfrac{h(\eta_{m-1}|a_{m-1},b_{m-1})}{h'(\eta_{m-1}|a_{m-1},b_{m-1})},\end{cases} \tag{45}$$

where p, p', q, q', and h are given in (31), (33), (32), (34), and (43), respectively. h' can be obtained by taking the derivative of (43) with respect to η_{m-1}, i.e.,

$$\begin{aligned}h'(\eta_{m-1}|a_{m-1},b_{m-1})=6N\eta_{m-1}^2+N(a_{m-1}^2+b_{m-1}^2)^2\\+2\left(3Na_{m-1}^2+3Nb_{m-1}^2-\|\boldsymbol{x}_r\|^2-\|\boldsymbol{x}_t\|^2\right)\eta_{m-1}\\-2\left(b_{m-1}^2\|\boldsymbol{x}_t\|^2+a^2\|\boldsymbol{x}_r\|^2-2a_{m-1}b_{m-1}|\boldsymbol{x}_t^\dagger\boldsymbol{x}_r|\right).\end{aligned} \tag{46}$$

3. If $|a_m-a_{m-1}|\le\epsilon$, $|b_m-b_{m-1}|\le\epsilon$ and $|\eta_m-\eta_{m-1}|\le\epsilon$, where ϵ is a preassigned parameter to control convergence, output $\hat{a}=a_m$, $\hat{b}=b_m$, and $\hat{\eta}=\eta_m$. Otherwise, repeat step 2 until convergence.

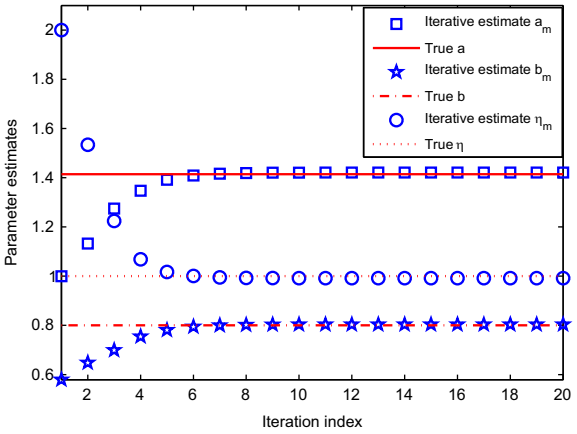

Fig. 2. Estimates of a_m, b_m and η_m for $M=100$, $N=100$, $a=\sqrt{2}$, $b=0.8$, and $\eta=1$.

It should be pointed out that Cyclic algorithm II might also be sensitive to the initial values of a, b, and η. Many numerical simulations conducted with Cyclic algorithm II imply that satisfactory solutions to (45) can be obtained in several iterations by initializing η as an arbitrary positive quantity and using the same initializations of a and b as those in the Cyclic algorithm I. As an example, one simulation result is presented in Fig. 2, where the initial value of η is set to be 2 and these curves are plotted by averaging over $M=100$ independent experiments.

After obtaining these MLEs under H_0 and H_1, one can insert them into (38). As a result, the GLRT detector for the stochastic model in (38) can be written as

$$L_2=\frac{\|\boldsymbol{x}_r\|^{2N}\|\boldsymbol{x}_t\|^{2N}}{\hat{\eta}^N(\hat{a}^2+\hat{b}^2+\hat{\eta})^N} \times\exp\left(\frac{-(\hat{b}^2+\hat{\eta})\|\boldsymbol{x}_t\|^2+(\hat{a}^2+\hat{\eta})\|\boldsymbol{x}_r\|^2-2\hat{a}\hat{b}|\boldsymbol{x}_t^{\dagger}\boldsymbol{x}_r|}{\hat{\eta}(\hat{a}^2+\hat{b}^2+\hat{\eta})}\right)\underset{H_0}{\overset{H_1}{\gtrless}}\gamma_4', \tag{47}$$

where γ_4' is a suitable modification version of threshold in (38).

4. Simulation results

In this section, simulation results are provided to illustrate the performance of the proposed GLRT detectors. For comparison purposes, the CC detector and the MF detector are considered. The CC detector T_{CC} is expressed as [15]

$$T_{\mathrm{CC}}=\left|\boldsymbol{x}_t^{\dagger}\boldsymbol{x}_r\right|^2\underset{H_0}{\overset{H_1}{\gtrless}}\gamma, \tag{48}$$

and the MF detector T_{MF} is [1]

$$T_{\mathrm{MF}}=\left|\boldsymbol{x}_t^{\dagger}\boldsymbol{s}\right|^2\underset{H_0}{\overset{H_1}{\gtrless}}\gamma. \tag{49}$$

Notice that the MF detector uses a priori knowledge about the transmitted signal $\boldsymbol{s}$, which is not available to all the other detectors. Therefore, the MF detector serves as a benchmark of the best possible performance in the presence of a noisy reference. For ease of comparison, analytical expressions for the probabilities of false alarm and detection of the CC detector and the MF detector are provided (see Appendices D and E). It should be pointed out that the high non-linearity of the proposed detectors leads to the difficulty in analytically assessing their detection performance. Hence, we use Monte Carlo (MC) techniques for the performance evaluation of the proposed detectors.

In the following, numerical simulations are given on the assumption that $s(n)$ for $n=0,\ldots,N-1$ are i.i.d. circular complex zero-mean Gaussian random variables with unit variance. Define the input SNR in the TC by

$$\mathrm{SNR}=10\log_{10}\frac{a^2}{\eta}, \tag{50}$$

and the input SNR in the RC by

$$\mathrm{SNR}_r=10\log_{10}\frac{b^2}{\eta}. \tag{51}$$

Note that these SNRs are defined at the *per-sample basis*. For simplicity, the GLRT detectors proposed in Section 3 for the stochastic model are referred to as Bayesian GLRT (B-GLRT) detectors, since a prior distribution is assumed on the transmitted waveform.

The detection probability curves of T_{CC} in (48) and T_{MF} in (49) are plotted with both the MC techniques and the corresponding analytical expressions in Fig. 3, where $N=100$, $\eta=0$ dB, $\mathrm{SNR}_r\in\{-10,0\}$ dB, and $P_{fa}=10^{-2}$. Note that the MF detector does not require the RC, and thus its performance is irrelevant to SNR_r. It can be seen that the results obtained by the analytical expressions match those obtained by the MC simulations pretty well. In addition, the detection performance of T_{CC} in (48) depends significantly on the SNR_r in the RC. The larger the SNR_r, the better the detection probability. The gap is about 8 dB at $P_d=0.9$ between the case of $\mathrm{SNR}_r=-10$ dB and the case of $\mathrm{SNR}_r=0$ dB. In particular, the MF detector T_{MF} provides an upper bound of detection performance. It can

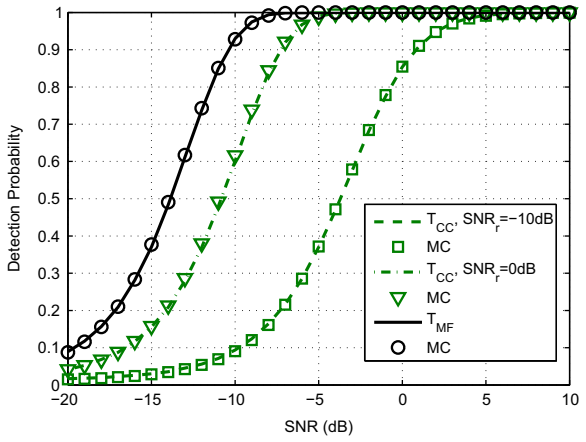

Fig. 3. P_d of T_{CC} (48) and T_{MF} (49) versus input SNR for $N=100$, $\eta=0$ dB, $\mathrm{SNR}_r\in\{-10,0\}$ dB, and $P_{fa}=10^{-2}$.

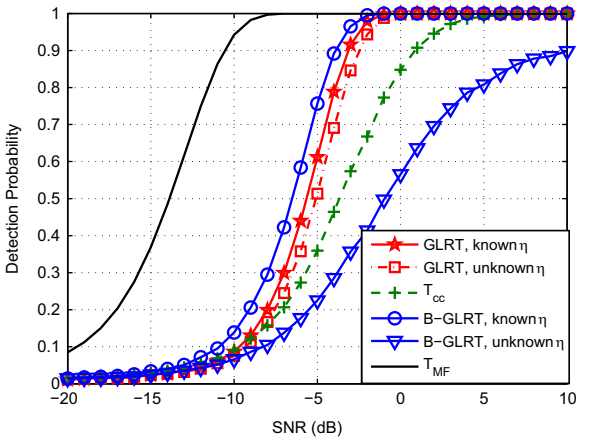

Fig. 4. P_d of T_{CC} (48), T_{MF} (49), GLRT (10) for known η, (19) for unknown η, B-GLRT (37) for known η and (47) for unknown η versus input SNR for $N=100$, $\eta=0$ dB, $\mathrm{SNR}_r=-10$ dB, and $P_{fa}=10^{-2}$.

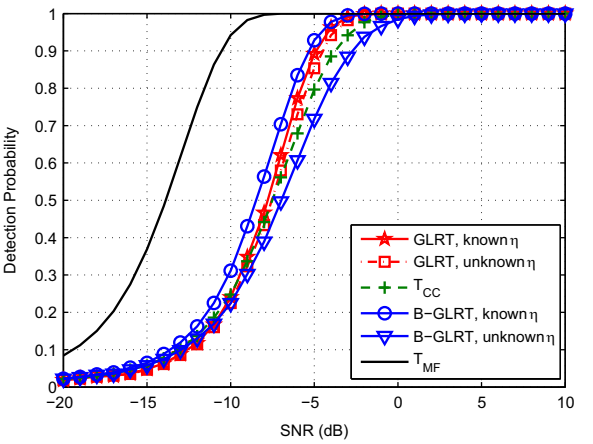

Fig. 5. P_d of T_{CC} (48) and T_{MF} (49), GLRT (10) for known η and (19) for unknown η, and the B-GLRT (37) for known η and (47) for unknown η versus input SNR for $N=100$, $\eta=0$ dB, $\mathrm{SNR}_r=-5$ dB, and $P_{fa}=10^{-2}$.

be observed that the gap at $P_d=0.9$ is about 3.1 dB between T_{CC} with $\mathrm{SNR}_r=0$ dB and T_{MF}.

The detection performance of the proposed GLRT detectors is presented in Fig. 4, where $\eta=0$ dB, $\mathrm{SNR}_r=-10$ dB, and $P_{fa}=10^{-2}$. Note that the detection probability curves of these detectors proposed in Sections 2 and 3 are evaluated with resorting to Monte Carlo (MC) techniques due to the non-availability of analytical expressions for the probabilities of false alarm and detection of these detectors. For comparison purposes, the CC detector T_{CC} in (48) and the MF detector T_{MF} in (49) are also provided. One can observe that the performance of the GLRT detectors in (10) and (19) is much better than that of T_{CC} for low SNR_r (e.g., $\mathrm{SNR}_r=-10$ dB in this example). The gap at $P_d=0.9$ is about 4 dB between detector (10) and T_{CC}, and is about 3.2 dB between detector (19) and T_{CC}. Interestingly, the B-GLRT detector in (37) outperforms the GLRT detector in (10) in the case of known η. However, the performance of the B-GLRT in (47) is much worse than that of the GLRT in (19) in the case of unknown η, and is even worse than that of T_{CC}.

In Figs. 5 and 6, we study the impact of different values of SNR_r on all the detectors considered. The other parameters are selected to be the same as in Fig. 4. Inspections of the two figures highlight that the value of SNR_r has an obvious influence on the detection performance of these detectors except the MF detector. The larger the SNR_r, the better the detection performance. The relationship among the detection performance of these detectors remains the same as in Fig. 4, but the performance differences become smaller and smaller when SNR_r increases. Particularly, the GLRT detectors, the B-GLRT detectors and T_{CC} almost have the same detection performance at $\mathrm{SNR}_r=0$ dB. The detection performance loss of these detectors with respect to T_{MF} is approximately 3 dB.

Note that the detection thresholds of the GLRT and B-GLRT with known noise variance η depend on the accuracy of the knowledge of η. In practice, the noise variance may be unknown and needs to be estimated. To consider the effect of the estimation error, denote by $\hat{\eta}=\varepsilon\eta$ the estimated noise power, where ε reflects how accurate the estimate is. Call $B=10\log_{10}\varepsilon$ the noise

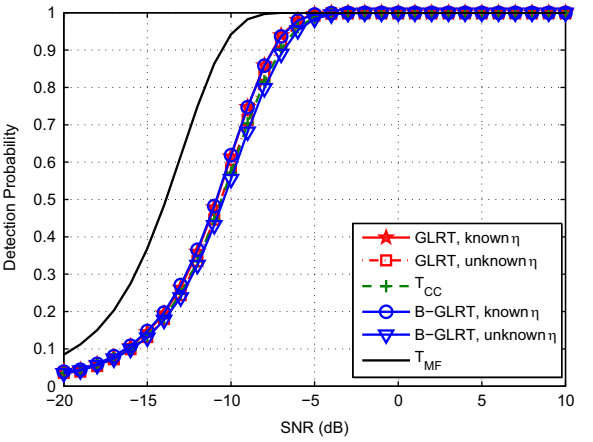

Fig. 6. P_d of T_{CC} (48) and T_{MF} (49), GLRT (10) for known η and (19) for unknown η, and the B-GLRT (37) for known η and (47) for unknown η versus input SNR for $N=100$, $\eta=0$ dB, $\mathrm{SNR}_r=0$ dB, and $P_{fa}=10^{-2}$.

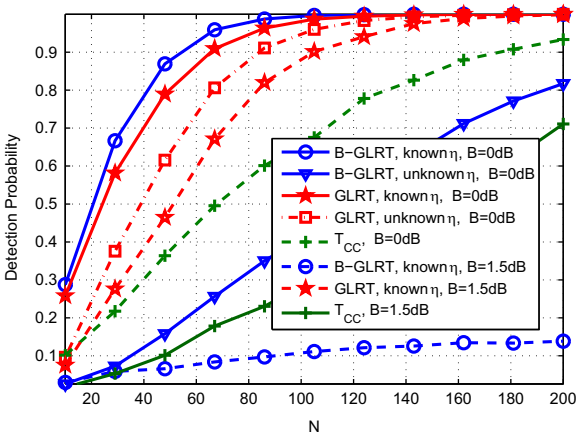

Fig. 7. P_d of GLRT, B-GLRT, and T_{CC} versus N for $P_{fa}=10^{-2}$, $\eta=0$ dB, $B\in\{0,1.5\}$ dB, $\mathrm{SNR}_r=-10$ dB, and $\mathrm{SNR}=-2$ dB.

uncertainty factor. In the following, we test the proposed detectors which employ the mismatched noise variance $\hat{\eta}$ to set the thresholds. The detection performance of the proposed detectors as a function of N (i.e., the number of samples) is illustrated for the mismatched case in Fig. 7, where $\mathrm{SNR}_r = -10$ dB and $\mathrm{SNR} = -2$ dB. It can be seen that each detector performs better as N increases. With perfectly known noise power (i.e., $B=0$ dB), the B-GLRT detector with known η performs the best, and the B-GLRT detector with unknown η provides the worst performance. However, for the mismatched case of $B=1.5$ dB, the performance of the CC, GLRT and B-GLRT detectors developed with known η degrades significantly. In particular, the GLRT with known η performs worse than the GLRT with unknown η in the current case. In addition, the CC and B-GLRT with known η give performance worse than the B-GLRT with unknown η.

5. Conclusions

In this paper, we have considered the two-channel detection problem with a noisy RC. In the model where the transmit signal is deterministic but unknown, two GLRT detectors are proposed with known and unknown noise power. For the transmit signal that can be approximated as a Gaussian process, two B-GLRT detectors with known and unknown noise power are developed by using cyclic iteration algorithms to find the MLEs of the unknown parameters. Due to the nonlinearity of the proposed detectors, theoretical analysis of these detectors is intractable. Their performance is assessed by MC simulations.

In our comparisons, we have included the conventional CC detector and the clairvoyant MF detector as benchmark. Simulation results demonstrate that the proposed four detectors except the one developed with unknown noise power in the stochastic model (i.e., the B-GLRT detector with unknown η) outperform the conventional CC detector, especially with low SNR_r in the RC. It is also shown that the performance of the B-GLRT detector with known η is better than that of the corresponding deterministic model based GLRT detector, and the MF detector provides an upper bound on the detection performance. However, in the presence of errors in the noise power estimate, the performance of the GLRT and B-GLRT with known η may degrade significantly. In addition, the detection performance of the proposed detectors highly depends on the SNR_r in the RC. The larger the SNR_r, the higher the detection probabilities. As the SNR_r increases, the performance difference between the proposed detectors and the MF detector becomes smaller.

Possible future research tracks include extending the framework to passive multistatic radar detection [25] as well as considering detection in signal-dependent clutter environments [26].

Appendix A. Proof of (8) and (9)

Using ℓ_1 defined in (6), we have

$$\max_{\{\alpha,\beta,\boldsymbol{s}\}} \ell_1 = \max_{\{\boldsymbol{s}\}}\left\{\max_{\{\alpha,\beta\}} \ell_1\right\}. \tag{52}$$

With a fixed $\boldsymbol{s}$, the MLEs of α and β in (52) are obtained as [25]

$$\hat{\alpha}_1 = \frac{\boldsymbol{s}^\dagger \boldsymbol{x}_t}{\boldsymbol{s}^\dagger \boldsymbol{s}} \quad \text{and} \quad \hat{\beta}_1 = \frac{\boldsymbol{s}^\dagger \boldsymbol{x}_r}{\boldsymbol{s}^\dagger \boldsymbol{s}}, \tag{53}$$

respectively. Substituting (53) into (52) yields

$$\max_{\{\boldsymbol{s}\}} \ell_1 = -2N \ln \pi - 2N \ln \eta - \frac{1}{\eta}\left(\|\boldsymbol{x}_r\|^2 + \|\boldsymbol{x}_t\|^2 - \max_{\{\boldsymbol{s}\}} \frac{\boldsymbol{s}^\dagger \mathbf{F}_1 \boldsymbol{s}}{\boldsymbol{s}^\dagger \boldsymbol{s}}\right), \tag{54}$$

where

$$\mathbf{F}_1 = \boldsymbol{x}_r \boldsymbol{x}_r^\dagger + \boldsymbol{x}_t \boldsymbol{x}_t^\dagger = \mathbf{X}\mathbf{X}^\dagger,$$

with $\mathbf{X} = [\boldsymbol{x}_r, \boldsymbol{x}_t]$. The maximization of (54) with respect to $\boldsymbol{s}$ is equivalent to maximizing the Rayleigh quotient $\boldsymbol{s}^\dagger \mathbf{F}_1 \boldsymbol{s} / \boldsymbol{s}^\dagger \boldsymbol{s}$. This maximum value is the largest eigenvalue of $\mathbf{F}_1$, i.e.,

$$\max_{\{\boldsymbol{s}\}} \frac{\boldsymbol{s}^\dagger \mathbf{F}_1 \boldsymbol{s}}{\boldsymbol{s}^\dagger \boldsymbol{s}} = \lambda_{\max}(\mathbf{F}_1) = \lambda_{\max}(\boldsymbol{\Phi}), \tag{55}$$

where $\boldsymbol{\Phi} = \mathbf{X}^\dagger \mathbf{X}$. Note that the employment of the 2-dimensional matrix $\boldsymbol{\Phi}$ instead of the N-dimensional matrix $\mathbf{F}$ in (55) is more computationally effective. The analytical solution to (55) is given by (see Appendix B)

$$\lambda_{\max}(\boldsymbol{\Phi}) = \frac{\|\boldsymbol{x}_t\|^2 + \|\boldsymbol{x}_r\|^2 + \sqrt{(\|\boldsymbol{x}_t\|^2 - \|\boldsymbol{x}_r\|^2)^2 + 4|\boldsymbol{x}_r^\dagger \boldsymbol{x}_t|^2}}{2}. \tag{56}$$

Substituting (56) into (54), we can obtain (8).

Similarly, ℓ_0 defined in (6) can be computed as

$$\max_{\{\beta,\boldsymbol{s}\}} \ell_0 = \max_{\{\boldsymbol{s}\}}\left\{\max_{\{\beta\}} \ell_0\right\}. \tag{57}$$

It is straightforward that the MLE of β under H_0 for a fixed $\boldsymbol{s}$ is given by

$$\hat{\beta}_0 = \frac{\boldsymbol{s}^\dagger \boldsymbol{x}_r}{\boldsymbol{s}^\dagger \boldsymbol{s}}. \tag{58}$$

Inserting (58) into (57) results in

$$\max_{\{\boldsymbol{s}\}} \ell_0 = -2N \ln \pi - 2N \ln \eta - \frac{1}{\eta}\left(\|\boldsymbol{x}_r\|^2 + \|\boldsymbol{x}_t\|^2 - \max_{\boldsymbol{s}} \frac{\boldsymbol{s}^\dagger \mathbf{F}_2 \boldsymbol{s}}{\boldsymbol{s}^\dagger \boldsymbol{s}}\right), \tag{59}$$

where $\mathbf{F}_2 = \boldsymbol{x}_r \boldsymbol{x}_r^\dagger$. It is easy to show that

$$\max_{\{\boldsymbol{s}\}} \frac{\boldsymbol{s}^\dagger \mathbf{F}_2 \boldsymbol{s}}{\boldsymbol{s}^\dagger \boldsymbol{s}} = \|\boldsymbol{x}_r\|^2. \tag{60}$$

Taking (60) into (59), we get (9).

Appendix B. The eigenvalues of matrix $\boldsymbol{\Phi}$

Obviously, $\boldsymbol{\Phi} = \mathbf{X}^\dagger \mathbf{X}$ can be expressed as

$$\boldsymbol{\Phi} = \begin{bmatrix} \|\boldsymbol{x}_r\|^2 & \boldsymbol{x}_r^\dagger \boldsymbol{x}_t \\ \boldsymbol{x}_t^\dagger \boldsymbol{x}_r & \|\boldsymbol{x}_t\|^2 \end{bmatrix}. \tag{61}$$

Denote by λ the eigenvalues of $\boldsymbol{\Phi}$. It follows that λ needs to satisfy the characteristic equation $c(\lambda, \boldsymbol{\Phi})$, i.e.,

$$c(\lambda, \boldsymbol{\Phi}) = \det\left(\lambda \mathbf{I} - \mathbf{X}^\dagger \mathbf{X}\right) = 0. \tag{62}$$

Substituting (61) into (62) produces

$$c(\lambda,\boldsymbol{\Phi})=\lambda^2-(\|\boldsymbol{x}_t\|^2+\|\boldsymbol{x}_r\|^2)\lambda+\|\boldsymbol{x}_r\|^2\|\boldsymbol{x}_t\|^2-|\boldsymbol{x}_t^\dagger\boldsymbol{x}_r|^2=0. \tag{63}$$

The solutions to (63) are

$$\lambda_1=\frac{\|\boldsymbol{x}_t\|^2+\|\boldsymbol{x}_r\|^2+\sqrt{(\|\boldsymbol{x}_t\|^2-\|\boldsymbol{x}_r\|^2)^2+4|\boldsymbol{x}_t^\dagger\boldsymbol{x}_r|^2}}{2},$$
$$\lambda_2=\frac{\|\boldsymbol{x}_t\|^2+\|\boldsymbol{x}_r\|^2-\sqrt{(\|\boldsymbol{x}_t\|^2-\|\boldsymbol{x}_r\|^2)^2+4|\boldsymbol{x}_t^\dagger\boldsymbol{x}_r|^2}}{2}. \tag{64}$$

Note that the 2-dimensional matrix $\boldsymbol{\Phi}$ only has two eigenvalues. Hence, the maximum and minimum eigenvalues are, respectively,

$$\lambda_{\max}(\boldsymbol{\Phi})=\lambda_1 \quad \text{and} \quad \lambda_{\min}(\boldsymbol{\Phi})=\lambda_2. \tag{65}$$

Appendix C. Proof of (31), (32), and (43)

Under H_1, the logarithm of $g_{H_1}^{\mathrm{s}}$ defined in (29) can be written as

$$\ln g_{H_1}^{\mathrm{s}}=-2N\ln\pi-N\ln\eta-N\ln\left(a^2+b^2+\eta\right)-\frac{(b^2+\eta)\|\boldsymbol{x}_t\|^2+(a^2+\eta)\|\boldsymbol{x}_r\|^2-2ab|\boldsymbol{x}_t^\dagger\boldsymbol{x}_r|}{\eta(a^2+b^2+\eta)}. \tag{66}$$

To obtain the MLEs of a, b, and η, let

$$\frac{\partial\ln g_{H_1}^{\mathrm{s}}}{\partial a}=0, \quad \frac{\partial\ln g_{H_1}^{\mathrm{s}}}{\partial b}=0, \quad \text{and} \quad \frac{\partial\ln g_{H_1}^{\mathrm{s}}}{\partial\eta}=0. \tag{67}$$

Substituting (66) into (67), we have

$$\frac{\partial\ln g_{H_1}^{\mathrm{s}}}{\partial a}=-\frac{2Na}{a^2+b^2+\eta}-\frac{2a\|\boldsymbol{x}_r\|^2-2b|\boldsymbol{x}_t^\dagger\boldsymbol{x}_r|}{\eta(a^2+b^2+\eta)}+2a\frac{(b^2+\eta)\|\boldsymbol{x}_t\|^2+(a^2+\eta)\|\boldsymbol{x}_r\|^2-2ab|\boldsymbol{x}_t^\dagger\boldsymbol{x}_r|}{\eta(a^2+b^2+\eta)^2}=0, \tag{68}$$

$$\frac{\partial\ln g_{H_1}^{\mathrm{s}}}{\partial b}=-\frac{2Nb}{a^2+b^2+\eta}-\frac{2b\|\boldsymbol{x}_t\|^2-2a|\boldsymbol{x}_t^\dagger\boldsymbol{x}_r|}{\eta(a^2+b^2+\eta)}+2b\frac{(b^2+\eta)\|\boldsymbol{x}_t\|^2+(a^2+\eta)\|\boldsymbol{x}_r\|^2-2ab|\boldsymbol{x}_t^\dagger\boldsymbol{x}_r|}{\eta(a^2+b^2+\eta)^2}=0, \tag{69}$$

and

$$\frac{\partial\ln g_{H_1}^{\mathrm{s}}}{\partial\eta}=-\frac{N}{\eta}-\frac{N}{a^2+b^2+\eta}-\frac{\|\boldsymbol{x}_t\|^2+\|\boldsymbol{x}_r\|^2}{\eta(a^2+b^2+\eta)}+\left(a^2+b^2+2\eta\right)\frac{(b^2+\eta)\|\boldsymbol{x}_t\|^2+(a^2+\eta)\|\boldsymbol{x}_r\|^2-2ab|\boldsymbol{x}_t^\dagger\boldsymbol{x}_r|}{\eta^2(a^2+b^2+\eta)^2}=0. \tag{70}$$

After some algebraic manipulations, (67) can be equivalently transformed to (42).

Appendix D. Performance analysis of CC detector

Proposition D.1. *Let* $\boldsymbol{s}=[s(0),s(1),\ldots,s(N-1)]^T$. *Assume that* $s(n)$, $n=0,\ldots,N-1$, *are i.i.d. circular complex zero-mean white Gaussian random variables with unit variance. For a large number of samples N, the probabilities of false alarm and detection of the CC detector in (48) are approximated as, respectively,*

$$P_{fa}=\exp\left\{-\frac{\gamma}{\sigma_{\mathrm{CC}_0}^2}\right\}, \tag{71}$$

and

$$P_d=Q_1\left(\sqrt{\frac{2|\mu_{\mathrm{CC}_1}|^2}{\sigma_{\mathrm{CC}_1}^2}},\sqrt{\frac{2\gamma}{\sigma_{\mathrm{CC}_1}^2}}\right), \tag{72}$$

where μ_{CC_1}, $\sigma_{\mathrm{CC}_1}^2$ *and* $\sigma_{\mathrm{CC}_0}^2$ *are given in (78), (79), and (80), respectively, and* $Q_m(a,b)$ *is the generalized Marcum Q-function of order m, i.e. [27, Eq. (4.33)]*

$$Q_m(a,b)=\int_b^\infty\frac{t^m}{a^{m-1}}\exp\left(-\frac{t^2+a^2}{2}\right)I_{m-1}(at)\,dt, \tag{73}$$

with $I_{m-1}(x)$ *denoting the modified Bessel function of the first kind of order* $m-1$, *i.e.*,

$$I_{m-1}(x)=\sum_{n=0}^{\infty}\frac{1}{n!\Gamma(m+n)}\left(\frac{x}{2}\right)^{2n+m-1}. \tag{74}$$

Proof. Let T'_{CC} be the CC operation between $\boldsymbol{x}_r$ and $\boldsymbol{x}_t$, i.e.,

$$T'_{\mathrm{CC}}=\boldsymbol{x}_t^\dagger\boldsymbol{x}_r=\sum_{n=0}^{N-1}x_t^\dagger(n)x_r(n), \tag{75}$$

where $\boldsymbol{x}_r=[x_r(0),x_r(1),\ldots,x_r(N-1)]^T$ and $\boldsymbol{x}_t=[x_t(0),x_t(1),\ldots,x_t(N-1)]^T$. According to the CLT [28], T'_{CC} with large N can be well approximated as a complex Gaussian random variable. Using (1), one can obtain that under H_1,

$$x_t^\dagger(n)x_r(n)=(\alpha s(n)+w(n))^\dagger(\beta s(n)+v(n))=\alpha^*\beta|s(n)|^2+\alpha^*s^*(n)v(n)+\beta s(n)w^*(n)+w^*(n)v(n). \tag{76}$$

It is easy to check that

$$E[x_t^\dagger(n)x_r(n)]=\alpha^*\beta,$$
$$\mathrm{var}(x_t^\dagger(n)x_r(n))=2a^2b^2+\eta b^2+a^2\eta+\eta^2. \tag{77}$$

Thus, the mean μ_{CC_1} and variance $\sigma_{\mathrm{CC}_1}^2$ of T'_{CC} under H_1 can be computed as, respectively,

$$\mu_{\mathrm{CC}_1}=N\alpha^*\beta, \tag{78}$$

and

$$\sigma_{\mathrm{CC}_1}^2=N(2a^2b^2+\eta b^2+a^2\eta+\eta^2). \tag{79}$$

Under H_0, the mean is zero, and the variance $\sigma_{\mathrm{CC}_0}^2$ is

$$\sigma_{\mathrm{CC}_0}^2=N(\eta b^2+\eta^2). \tag{80}$$

As a result, the false alarm probability of the CC detector T_{CC} in (48) can be computed as

$$P_{fa}=\Pr(T_{\mathrm{CC}}\geq\gamma|H_0)=\Pr\left(\frac{|T'_{\mathrm{CC}}|^2}{\sigma_{\mathrm{CC}_0}^2}\geq\frac{\gamma}{\sigma_{\mathrm{CC}_0}^2}\middle|H_0\right). \tag{81}$$

It can be shown that $|T'_{\mathrm{CC}}|^2/\sigma_{\mathrm{CC}_0}^2$ is a complex central Chi-square random variable with 1 degree of freedom (DOF) [29, Appendix A]. Hence, P_{fa} in (71) can be obtained. Moreover, the detection probability of the CC detector in

(48) can be expressed as

$$P_d = \Pr(T_{CC} \geq \gamma | H_1) = \Pr\left(\frac{|T'_{CC}|^2}{\sigma^2_{CC_1}} \geq \frac{\gamma}{\sigma^2_{CC_1}} \middle| H_1 \right), \tag{82}$$

where $|T'_{CC}|^2/\sigma^2_{CC_1}$ is a complex non-central Chi-square random variable with 1 DOF and non-centrality parameter $\lambda_{CC_1} = |\mu_{CC_1}|^2/\sigma^2_{CC_1}$. Thus, P_d in (72) can be derived. □

Note that the generalized Marcum function $Q_m(a,b)$ can be easily computed by the most popular computing softwares with built-in routines, e.g., the function *marcumq (a,b,m)* in MATLAB.

Appendix E. Performance analysis of MF detector

The analytical expressions for the probabilities of false alarm and detection of the MF detector with deterministic $\boldsymbol{s}$ are available in [1,30]. The following proposition offers the counterpart by assuming $\boldsymbol{s}$ to be random.

Proposition E.1. *Assume that $s(n)$, $n = 0, \ldots, N-1$, are i.i.d. circular complex zero-mean white Gaussian random variables with unit variance. For large N, the probabilities of false alarm and detection of the MF detector given in (49) can be approximated as, respectively,*

$$P_{fa} = \exp\left\{ -\frac{\gamma}{\sigma^2_{MF_0}} \right\}, \tag{83}$$

and

$$P_d = Q_1\left(\sqrt{\frac{2|\mu_{MF_1}|^2}{\sigma^2_{MF_1}}}, \sqrt{\frac{2\gamma}{\sigma^2_{MF_1}}} \right), \tag{84}$$

where $\sigma^2_{MF_0}$ and μ_{MF_1} along with $\sigma^2_{MF_1}$ are given in (86) and (87), respectively.

Proof. Let T'_{MF} be the CC operation between $\boldsymbol{x}_t$ and $\boldsymbol{s}$, i.e.,

$$T'_{MF} = \boldsymbol{x}_t^\dagger \boldsymbol{s} = \sum_{n=0}^{N-1} x_t^\dagger(n) s(n). \tag{85}$$

Due to the CLT, T'_{MF} for large N under H_0 can be approximated as a complex zero-mean Gaussian random variable with variance

$$\sigma^2_{MF_0} = N\eta. \tag{86}$$

Similarly, T'_{MF} under H_1 can be approximated as a complex Gaussian random variable whose mean μ_{MF} and variance $\sigma^2_{MF_1}$ are given by, respectively,

$$\mu_{MF_1} = N\alpha^* \quad \text{and} \quad \sigma^2_{MF_1} = N(2a^2 + \eta). \tag{87}$$

Hence, P_{fa} can be expressed as

$$P_{fa} = \Pr(T_{MF} \geq \gamma | H_0) = \Pr\left(\frac{|T'_{MF}|^2}{\sigma^2_{MF_0}} \geq \frac{\gamma}{\sigma^2_{MF_0}} \middle| H_0 \right), \tag{88}$$

where $|T'_{MF}|^2/\sigma^2_{MF_0}$ is a complex central Chi-square random variable with 1 DOF [29, Appendix A]. Thus, P_{fa} in (83) can be obtained. Moreover, P_d can be expressed as

$$P_d = \Pr(T_{MF} \geq \gamma | H_1) = \Pr\left(\frac{|T'_{MF}|^2}{\sigma^2_{MF_1}} \geq \frac{\gamma}{\sigma^2_{MF_1}} \middle| H_1 \right), \tag{89}$$

where $|T'_{MF}|^2/\sigma^2_{MF_1}$ is a complex non-central Chi-square random variable with 1 DOF and non-centrality parameter $\lambda_{MF_1} = |\mu_{MF_1}|^2/\sigma^2_{MF_1}$. Thus, P_d in (84) can be derived. □

References

[1] S.M. Kay, Fundamentals of Statistical Signal Processing, Volume II: Detection Theory, Prentice-Hall, Upper Saddle River, NJ, 1998.
[2] G.C. Carter, Coherence and time delay estimation, Proc. IEEE 75 (February (2)) (1987) 236–255.
[3] S. Stein, Differential delay/Doppler ML estimation with unknown signals, IEEE Trans. Signal Process. 41 (August (8)) (1993) 2717–2719.
[4] B. Xerri, J.-F. Cavassilas, B. Borloz, Passive tracking in underwater acoustic, Signal Process. 82 (August (8)) (2002) 1067–1085.
[5] B.A. Yocom, B.R. La Cour, T.W. Yudichak, A Bayesian approach to passive sonar detection and tracking in the presence of interferers, IEEE J. Ocean. Eng. 36 (July (3)) (2011) 386–405.
[6] L.C. Wood, S. Treitel, Seismic signal processing, Proc. IEEE 63 (April (4)) (1975) 649–661.
[7] D. Draganov, K. Wapenaar, J. Thorbecke, Seismic interferometry: reconstructing the earths reflection response, Geophysics 71 (July (4)) (2006) SI61–SI70.
[8] B. Artman, Imaging passive seismic data, Geophysics 71 (July (4)) (2006) SI117–SI187.
[9] A. Roueff, P. Roux, P. Refregier, Wave separation in ambient seismic noise using intrinsic coherence and polarization filtering, Signal Process. 89 (April (4)) (2009) 410–421.
[10] E. Pereda, R.Q. Quiroqa, J. Bhattacharya, Nonlinear multivariate analysis of neurophysiological signals, Prog. Neurobiol. 77 (2005) 1–37.
[11] W. Muhammad, O. Mester, H. Rix, D. Farina, A pseudopoint estimation of time delay and scale factor for M-wave analysis, IEEE Trans. Biomed. Eng. 50 (April (4)) (2003) 459–468.
[12] J. Garnier, G. Papanicolaou, Passive sensor imaging using cross correlations of noisy signals in a scattering medium, SIAM J. Imaging Sci. 2 (2) (2009) 396–437.
[13] L. Wang, B. Yazici, Passive imaging of moving targets using sparse distributed apertures, SIAM J. Imaging Sci. 5 (3) (2012) 769–808.
[14] H.D. Griffiths, C.J. Baker, Passive coherent location radar systems. Part 1: performance prediction, IEE Proc. Radar Sonar Navig. 152 (June (3)) (2005) 124–132.
[15] P.E. Howland, D. Maksimiuk, G. Reitsma, FM radio based bistatic radar, IEE Proc. Radar Sonar Navig. 152 (June (3)) (2005) 107–115.
[16] L. Wang, C.E. Yarman, B. Yazici, Doppler-hitchhiker: a novel passive synthetic aperture radar using ultranarrowband sources of opportunity, IEEE Trans. Geosci. Remote Sens. 49 (October (10)) (2011) 3521–3537.
[17] Digital Video Broadcasting (DVB): Frame Structure Channel Coding and Modulation for a Second Generation Digital Terrestrial Television Broadcasting System (DVB-T2), Technical Report ETSI-EN-302-755-V1.1.1, European Telecommunications Standards Institute, France, September 2009.
[18] M. Steiner, K. Gerlach, Fast convergence adaptive processor or a structured covariance matrix, IEEE Trans. Aerosp. Electron. Syst. 36 (October (4)) (2000) 1115–1126.
[19] P. Paysarvi-Hoseini, N.C. Beaulieu, Optimal wideband spectrum sensing framework for cognitive radio systems, IEEE Trans. Signal Process. 59 (March (3)) (2011) 1170–1182.
[20] D.E. Hack, L.K. Patton, B. Himed, M.A. Saville, Detection in passive MIMO radar networks, IEEE Trans. Signal Process. 62 (June (11)) (2014) 2999–3012.
[21] K. Polonen, V. Koivunen, Detection of DVB-T2 control symbols in passive radar systems, in: Proceedings of 2012 IEEE 7th Sensor Array and Multichannel Signal Processing Workshop (SAM), Hoboken, NJ, USA, June 2012, pp. 309–312.
[22] C.Y. Chen, P.P. Vaidyanathan, MIMO radar waveform optimization with prior information of the extended target and clutter, IEEE Trans. Signal Process. 57 (September (9)) (2009) 3533–3544.
[23] A. Aubry, A. De Maio, A. Farina, M. Wicks, Knowledge-aided (potentially cognitive) transmit signal and receive filter design in signal-dependent clutter, IEEE Trans. Aerosp. Electron. Syst. 49 (January (1)) (2013) 93–117.
[24] S.M. Kay, Fundamentals of Statistical Signal Processing, Volume I: Estimation Theory, Prentice-Hall, Upper Saddle River, NJ, 1998.
[25] K.S. Bialkowski, I.V.L. Clarkson, S.D. Howard, Generalized canonical correlation for passive multistatic radar detection, in: Proceedings of

2011 IEEE Statistical Signal Processing Workshop (SSP), Nice, France, June 2011, pp. 417–420.
[26] F. Colone, R. Cardinali, P. Lombardo, Cancellation of clutter and multipath in passive radar using a sequential approach, in: Proceedings of 2006 IEEE Conference on Radar, Verona, NY, USA, April 2006, pp. 393–399.
[27] M.K. Simon, M.-S. Alouini, Digital Communications over Fading Channels: A Unified Approach to Performance Analysis, John Wiley & Sons, Inc., New York, 2000.
[28] J.A. Rice, Mathematical Statistics and Data Analysis, 3rd ed. Duxbury Press, Belmont, CA, USA, 2007.
[29] C.D. Richmond, Performance of the adaptive sidelobe blanker detection algorithm in homogeneous environments, IEEE Trans. Signal Process. 48 (May (5)) (2000) 1235–1247.
[30] K.J. Sohn, H. Li, B. Himed, Parametric Rao test for multichannel adaptive signal detection, IEEE Trans. Aerosp. Electron. Syst. 43 (July (3)) (2007) 920–933.